

## ∂LITE: Differentiable Lighting-Informed Trajectory Evaluation for On-Orbit Inspection

Jack Naylor<sup>ID 1\*</sup>, Raghav Mishra<sup>ID 1,2</sup>, Nicholas H. Barbara<sup>ID 1</sup>, and Donald G. Dansereau<sup>ID 1,2</sup>

<sup>1</sup>Australian Centre for Robotics and School of Aerospace, Mechanical and Mechatronic Engineering, The University of Sydney, NSW, 2006, Australia

<sup>2</sup>Australian Robotic Inspection and Asset Management (ARIAM) Hub, The University of Sydney, NSW, 2006, Australia

\* Corresponding Author. Email: jack.naylor@sydney.edu.au

### Abstract

Visual inspection of space-borne assets is of increasing interest to spacecraft operators looking to plan maintenance, characterise damage, and extend the life of high-value satellites in orbit. The environment of Low Earth Orbit (LEO) presents unique challenges when planning inspection operations that maximise visibility, information, and data quality. Specular reflection of sunrays from spacecraft bodies, self-shadowing, and dynamic lighting in LEO significantly impact the quality of data captured throughout an orbit. This is exacerbated by the relative motion between spacecraft, which typically introduces variable imaging distances and attitudes during inspection. Planning inspection trajectories via simulation is a common approach. However, the ability to design and optimise an inspection trajectory specifically for the resulting quality of imaging data in proximity operations remains largely unexplored. In this work, we present ∂LITE, an end-to-end differentiable simulation pipeline for on-orbit inspection operations. We leverage state-of-the-art differentiable rendering tools and a custom orbit propagator to enable end-to-end optimisation of orbital parameters based on visual measurements. ∂LITE enables us to optimise for non-obvious trajectories, vastly improving the quality and usefulness of attained data. To our knowledge, our differentiable inspection-planning pipeline is the first of its kind and provides new insights into modern computational approaches to spacecraft mission planning.

### 1. Introduction

As the number and value of assets in space rapidly increases, there is a growing need for reliable and efficient visual inspection capabilities in orbit. Spacecraft operators can use inspection data to assess damage, plan maintenance, and extend the operational lifespan of high value satellites. However, conducting visual inspections in Low Earth Orbit (LEO) presents a unique set of challenges. The dynamic lighting conditions caused by specular reflections, self-shadowing, and the rapid orbital motion of spacecraft can significantly degrade image quality and limit the visibility of key features [1]. Moreover, the relative motion between inspection and target spacecraft introduces variability in imaging distance and orientation, further complicating data acquisition.

Historically, on-orbit inspection and servicing of spacecraft in LEO has been performed manually to return high-value assets to service [2, 3], and to extend mission life and capability [4–7]. Autonomous on-orbit inspection, however, is a more recent capability. Demonstrator missions for proximity operations like Orbital Express [8], precision formation-flying missions like PROBA-3 [9], and emerging servicing missions like Northrup Grum-

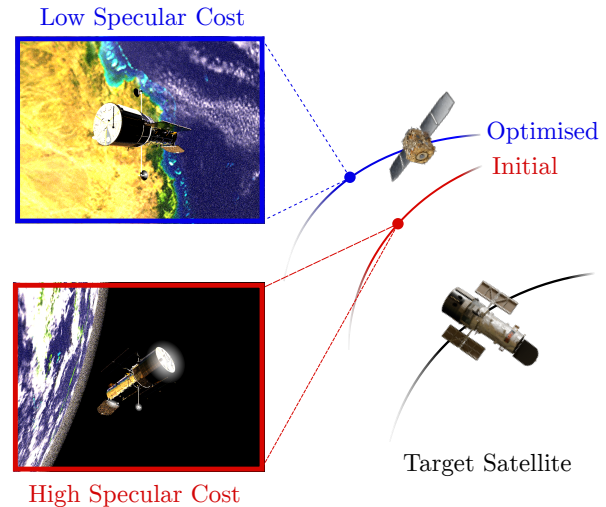


Fig. 1. ∂LITE is an end-to-end differentiable simulator for on-orbit inspection which produces non-obvious trajectories based on visual costs. We optimise orbital parameters for passive inspection trajectories that yield superior quality images of a target satellite by minimising specular reflections seen by the sensor.

man's Mission Extension Vehicle (MEV) [10], have demonstrated key capabilities relied upon to achieve on-orbit servicing. Planning informative inspections which attain high-fidelity visual data to inform these servicing operations remains a challenge.

Inspection and rendezvous missions in high Earth orbits such as Geostationary Orbit (GEO) [11] benefit from sustained illumination and often slow relative dynamics, allowing for predictable imaging of target spacecraft. In contrast, inspection in LEO has varying imaging geometries owing to stronger orbital perturbations, highly dynamic lighting environments, and rapid relative motion vastly complicating the inspection of satellites. Techniques for long-range imaging of satellites in LEO [12] are more resilient to such complicating factors, but they are unable to characterise damage and component level failure in the resolution needed to plan servicing operations. To enable related operations like docking and state estimation of satellites, alternate imaging modalities like event cameras [13, 14] have been proposed to handle imaging in changing lighting conditions with High Dynamic Range (HDR). However, such methods require substantial processing to provide the visual information to perform change detection, damage characterisation, and 3D reconstruction for repair and servicing operations compared to traditional imaging.

While simulation-based trajectory planning is common practice for on-orbit inspection, current methods overlook the impact of lighting conditions on the quality of imaging data. To address this gap, we introduce  $\partial$ LITE—a novel, end-to-end differentiable simulation pipeline specifically designed for visual on-orbit inspection planning. By integrating state-of-the-art differentiable rendering techniques with a differentiable orbit propagator,  $\partial$ LITE enables the optimisation of inspection trajectories based on visual measurements, allowing the user to refine orbital paths to improve relative lighting conditions, and ultimately the fidelity of collected data. To our knowledge,  $\partial$ LITE represents the first fully differentiable framework for planning visual inspection trajectories in space.

Our main contributions are as follows:

- We propose  $\partial$ LITE, a fully differentiable simulator, combining a custom, fully-differentiable implementation of the SGP4 orbital propagator [15] with a photometrically accurate differentiable renderer built with the Mitsuba 3 rendering engine [16];
- We demonstrate end-to-end optimisation of inspection orbits to minimise visual costs associated with blinding specular reflections using gradient-based optimisation; and

- We show that our optimised orbits improve other proxy metrics for close range satellite operations such as the number of visual features detected over the trajectory.

We envisage that  $\partial$ LITE will enable simpler trajectory planning with favourable trajectories in on-orbit inspection missions. More broadly, we anticipate our pipeline will underpin the development of future planning approaches that are *appearance-aware* and consider complex visual appearance including specularity [17], shadowing [18], and self-occlusion. Such approaches consider the quality of visual information captured, which is critical under the time, resource, and cost constraints of satellite missions compared to traditional visibility [19, 20] and coverage-based planning methods [21, 22].

## 2. Background

$\partial$ LITE combines orbital simulation with a high-fidelity visual simulation of satellite observations. Existing pipelines for simulation-based inspection planning typically focus only on simulating sensor data [23], dataset generation for pose estimation and navigation [24], or existing mission trajectories without optimisation [25, 26]. While tools such as SISPO [25] do include complex visual effects such as optical distortion and rendering of custom point spread functions, they do not allow direct computational design of orbits. To enable direct optimisation of orbital parameters, we develop  $\partial$ LITE with fully differentiable photorealistic rendering and orbital propagation. We compare the capabilities of prior works with  $\partial$ LITE in Table 1.

In the following subsections, we provide a brief overview of relevant background on Non-Earth Imaging

Table 1. Comparison of visual simulation frameworks for on-orbit inspection missions.  $\partial$ LITE is an end-to-end differentiable, photometrically accurate simulator which can produce photorealistic renderings of observations from an inspection satellite. Green indicates full capabilities, yellow indicates partial capability, and red indicates no capability.

Name	Diff. Orbits	Diff. Rendering	Photometric	Optical Effects	Photorealistic
ALL-STAR [26]					Yellow
SPIN [24]	Red				
SISPO [25]		Yellow	Green		
HySim [23]	Red	Yellow	Green	Yellow	
$\partial$ LITE (Ours)	Green	Green	Green	Yellow	Green

(NEI), orbital trajectory planning, differentiable programming, and differentiable scene rendering, which form the core elements of  $\partial$ LITE.

### 2.1 Non-Earth Imaging

Recent advances in NEI have allowed for high quality classification and characterisation of space objects using visual imagery. Private organisations such as Maxar Technologies and HEO [27] have demonstrated these capabilities commercially using fly-by NEI, whereby satellites are tasked with capturing high resolution images of target objects. This data allows for visual identification of objects from a distance, including satellites, discarded rocket bodies, and other unknown objects in LEO [12].

Most recently, Astroscale's ADRAS-J mission [28] has demonstrated sustained, high-resolution inspection of non-cooperative debris in close proximity. By taking images of a H-IIA upper stage rocket body, they provided insight into features of the target craft such as its attitude dynamics, and ultraviolet degradation of its thermal insulation, thereby informing future missions to capture and de-orbit the debris. However, owing to the dynamic illumination and relative motion in orbit, the quality of captured imagery varies significantly during an orbit, creating blinding reflections and HDR conditions which are difficult to extract useful insight from (Fig. 2).

In this work, we consider similar close proximity inspection missions. However, we focus on optimising orbital trajectories to maximise the quality of all images captured during an inspection, thereby avoiding events such as that shown in Fig. 2.



Fig. 2. Images of an H-IIA upper stage rocket body captured by Astroscale's ADRAS-J mission [28]. The mission was able to capture high-quality images of the rocket body over much of its inspection orbit (left). However, lens flares due to specular reflections make some images uninformative (right).

### 2.2 Orbital Trajectory Planning

Orbital trajectory optimisation is widely used when planning interplanetary trajectories [29–31], navigating through complex gravitational zones with many interacting perturbations [32], for manoeuvres transferring between orbits [33], and for managing swarms of inspection spacecraft [34]. This technique includes a rich literature of trajectory optimisation for terrestrial applications, such as in robotics [35–37]. In the context of astrodynamics, the trajectory of a spacecraft is numerically optimised by computing the thrust forces and/or attitude for a given objective function to be maximised.

For inspection tasks, one must design orbital trajectories that maintain an appropriate distance to and view of the target satellite. A typical strategy when designing close-proximity inspection orbits for a given target satellite is to make use of the periodic relative motion that naturally occurs between two spacecraft in similar orbits. For example, if the target is in a circular orbit, and the orbit of the inspection spacecraft is identical except for a small change in eccentricity, then the relative motion of the inspector with respect to the target is elliptical (i.e., a football orbit [38]). This allows the inspector to view the target from a range of different angles simply by leveraging the passive orbital dynamics of the two bodies.

Common inspection orbits [38] are chosen to maximise coverage of the target—or a specific site of interest on the target—in the relative frame, ensuring that sufficient image data can be captured over multiple passes. If, however, one wishes to impose more sophisticated design criteria on the inspection orbit, then more sophisticated orbital trajectory optimisation is required.

### 2.3 Differentiable Programming

One approach to performing trajectory optimisation is to leverage modern advances in differentiable programming [39]. Differentiable programming languages [40] and libraries [41] allow users to write code that is automatically differentiable—that is, gradients of functions and other operations can be automatically and efficiently computed without the user having to explicitly define them. Writing algorithms in a differential programming package enables usecases in optimising inputs, outputs, or algorithm parameters for computational design, model learning, uncertainty propagation, sensitivity analysis, and much more. This simple and flexible framework makes it easy for users to optimise arbitrary objective functions with first-order optimisation schemes (e.g., gradient descent), and has led to its widespread use in optimisation [37, 42] and machine learning [43, 44]. More recently, differentiable physics engines [45–47] and render-

ers [48, 49] have emerged, allowing for gradient propagation through complex physical environments.

#### 2.4 Differentiable Rendering for Downstream Tasks

Differentiable rendering engines are able to render a 3D scene and calculate gradients and Jacobian-vector products of the output with respect to scene parameters. This allows (for example) one to optimise for parameters in the scene such as camera or object poses, textures, surface normals, and more using gradient based optimisation. Ray-based differentiable rendering pipelines like Mitsuba 3 [16] enable complex lighting effects like interreflection, occlusion, self-shadowing, and scattering to be represented which are physically based [50] compared to rasterisation-based methods [51]. HDR environments with reflective scene elements, like those found in space [13, 52], produce complex visual appearances most accurately represented with physically-based ray tracing.

Increasingly in robotics, creating data for training agents with methods such as reinforcement learning [43] requires not only physically accurate dynamics [53] but also visually accurate scenes [46, 54] which minimise the domain gap between simulation and deployment in downstream tasks. In particular, differentiable photorealistic representations of a robot's environment enabled by new scene representations [55] have enabled downstream tasks from pose optimisation, odometry and trajectory planning [56, 57]. We take a similar approach in this work.

### 3. Method

We create a simulation environment combining differentiable rendering with a differentiable orbit propagator, allowing for high fidelity ray-traced renderings with photorealistic appearance based on accurate models of orbital dynamics. Combining both of these components, our  $\partial$ LITE pipeline can perform non-trivial optimisation of orbital elements from costs associated with visual observations.

#### 3.1 Trajectory Optimisation Approach

We pose the visual inspection planning problem in a trajectory optimisation framework. We assume the target spacecraft is cooperative, its orbital parameters are known, and that it has an accurate 3D model available for use during planning. We directly optimise a set of orbital parameters for the chaser,  $o_c$ , as decision variables to minimise a cost on a visual imaging model of the spacecraft. We implement trajectory optimisation by combining SGP4, an orbit propagator, with a differentiable renderer.

As the imaging process is continuous, to make it tractable, we discretise the trajectory by sampling evenly-

spaced points over a time period. We consider  $N$  evenly spread snapshots over a time period  $t \in [0, T]$ .

The final trajectory optimisation problem to find ideal orbital parameters can be written as

$$\begin{aligned} \min_{o_c} \quad & \sum_{i=0}^N \lambda_S \mathcal{L}_S(\mathcal{I}(t_i)) + \lambda_d \mathcal{L}_d(r_c(t_i), r_t(t_i)) \\ \text{s.t. } \mathcal{I}(t_i) &= \text{Render}(r_c(t_i), r_t(t_i), t_i) \\ r_c(t) &= \text{SGP4}(t_i, o_c) \\ r_t(t) &= \text{SGP4}(t_i, o_t) \\ t_i &= i \frac{T}{N} \end{aligned}$$

where  $o_c$  is the set of chaser orbital elements to optimise over, SGP4( $\cdot$ ) is our orbit propagator (Section 3.2), Render( $\cdot$ ) is our renderer (Section 3.3), and  $\mathcal{L}_S$  and  $\mathcal{L}_d$  are our specular intensity and distance regulariser cost functions respectively (Section 3.4).  $T$  is a period of time we want to optimise over, and  $\lambda_S$  and  $\lambda_d$  are weights that trade off between the two cost terms.

We perform gradient-based optimisation using the Adam optimiser with a learning rate of  $4 \times 10^{-6}$  to optimise the cost. We optimise for 200 iterations and empirically find it generally converges in less than 150 iterations with our choice of cost functions and optimisation parameters. For our experiments, we choose  $o_c = \{i_c, M_c, e_c\}$  which are the inclination, mean anomaly, and the eccentricity respectively. However, any physical parameters that are used as input for orbit propagation can be optimised if desired for a given task.

We initialise the inspection craft in an identical orbit to the target satellite except for a small shift in the initial mean anomaly to put it in a periodic circular relative orbit to the target as each target is already in an approximately circular orbit. We initialise the mean anomaly of the chaser,  $M_c$ , in terms of the target mean anomaly,  $M_t$  as

$$M_c = M_t - \frac{d}{a_t},$$

where  $d$  is the desired radius of the relative circular motion, and  $a_t$  is the semi-major axis. Note that  $\partial$ LITE is compatible with any initial inspection orbit—we simply chose a circular orbit for illustrative purposes. A review of common types of inspection orbit designs can be found in [38].

#### 3.2 Differentiable Orbit Propagation

Numerical algorithms for orbit propagation pose a problem for computational design of orbits as derivatives of objective functions with respect to design variables are not easily expressed. This hampers the use of traditional

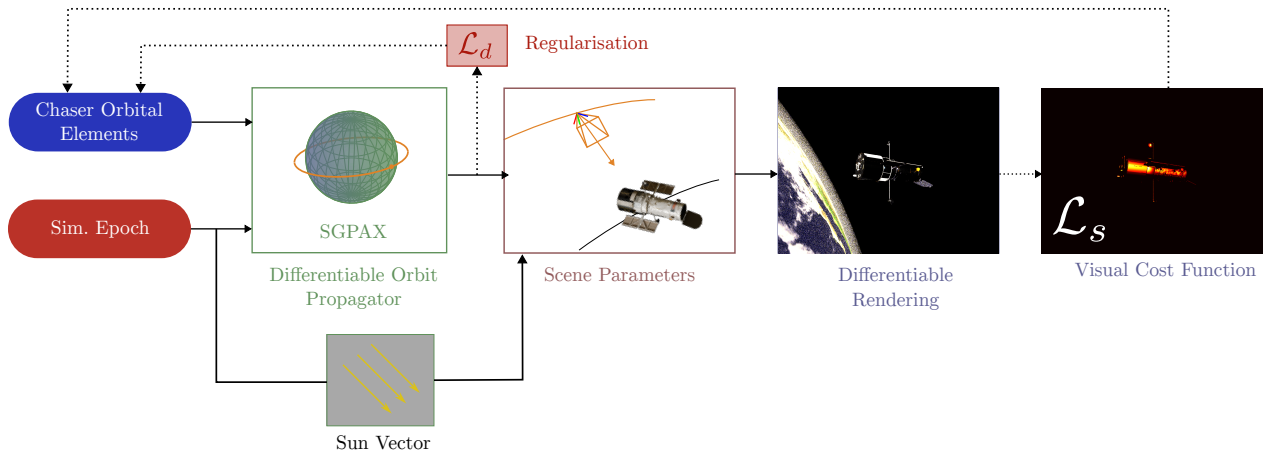


Fig. 3. An overview of the  $\partial$ LITE pipeline. Given a TLE for the chaser satellite and a simulation epoch, we compute a time-varying sun vector  $\hat{\mathbf{l}}$ , and satellite position at time  $t$ . The scene parameters are updated to produce rendered inspection imagery. From these observations we formulate a visual cost  $\mathcal{L}_s$  capturing the specularity in the scene to backpropagate gradients through the pipeline (dotted lines).

gradient-based algorithms, and has resulted in the use of black-box metaheuristic algorithms in astrodynamics such as genetic algorithms for computational design [58].

Using differentiable programming, along similar lines as [59], we implement `sgpax`—an implementation of the SGP4 orbit propagator [60] which is a general perturbation based propagator that works directly with Two Line Elements (TLEs). We implement `sgpax` with the JAX [41] differential programming package, giving us the ability to take arbitrary analytical derivatives between variables through auto differentiation in the forward and reverse mode. Our code is based on the implementation in [15, 61] and follows the programming interface of the open source python-sgp4 package [62]. `sgpax` is therefore a drop-in replacement for standard SGP4 propagators, allowing for effortless integration with other differentiable pipelines.

Our SGP4 implementation is easily parallelised and can be run on Graphics Processing Units (GPUs) or tensor processing units. This facilitates the use of large-scale Monte Carlo simulations, probabilistic inference, and applications in machine learning. Compared to [59], the JAX backend provides a drop-in NumPy interface, better support for forward-mode automatic differentiation, and native auto-parallelisation support for Monte Carlo simulations, which are common in space mission planning.

### 3.3 Photometrically Accurate Orbital Simulation

Given the dynamic range and intensity of illumination in LEO, photometrically accurate renderings are of key relevance when developing inspection missions [13, 52]. Taking advantage of the spectral rendering capabil-

ities of Mitsuba 3 [16], we introduce a directional light source with spectral irradiance consistent with captured data [63]. The scene scale is in meters, providing radiometric intensity at the sensor in units of Watts per meter per steradian. While we focus this work on visual inspection, adjustments to the sensor spectral sensitivity would allow  $\partial$ LITE to simulate inspections from sensors with different responses including infrared, multispectral, or hyperspectral cameras [23].

$\partial$ LITE models dynamic lighting directions at each inspection point. The sun direction vector  $\hat{\mathbf{l}}$  is defined as the negative unit vector towards the subsolar point, the point on the Earth with normal vector to the sun at the current orbital position and rotation of the Earth. This is computed using the solar azimuth [64], based on the Equation of Time [65] to compute this point in Earth-Centred-Earth-Fixed coordinates. As these relations are defined by trigonometric polynomials and related to the Julian Day of the simulation, it is possible to pass gradients through the lighting vector, enabling non-obvious optimisation of orbital phasing.

A photorealistic model of the Earth was constructed with a custom Bi-directional Scattering Distribution Function (BSDF). Textures for the BSDF were taken from the NASA Blue Marble: The Next Generation [66] dataset and constructed to produce a similar Earthshine intensity, for accurate reflections of the background on the surface of the spacecraft. To match the visual complexity of the background, both the presence of clouds and atmospheric scattering are simulated at realistic altitudes.

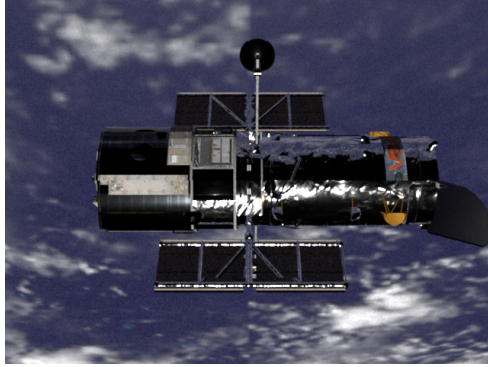


Fig. 4. Simulated observation from our photometrically accurate simulation. Including photorealistic Earth models alongside representative visual models of a satellite,  $\partial$ LITE produces high fidelity visual simulations of satellites in orbit.

Images are rendered using a path replay backpropagation integrator suitable for handling volumetric scattering from the atmosphere [67] and allowing derivatives to pass from cost maps in the image space back through poses of the camera and target satellite for optimisation. As the captured images are in radiometric units, we use a simplified sensor model to simulate them. This is required to be calibrated for a particular sensor, so for simplicity in our pipeline this is approximated using standard radiance-to-image plane transformations [68] and indicative electron conversions to form digital numbers at the sensor. This component of our pipeline can be heavily customised to test custom image signal processing approaches and HDR imaging methods. An example image from our pipeline is shown in Figure 4.

### 3.4 Optimising for Imaging Conditions

To demonstrate the capability of  $\partial$ LITE, we show an example of how it may be used to improve imaging conditions in the context of bright specular reflections which are common in orbit. We emphasise that  $\partial$ LITE is not limited to this application, as it gives the user the flexibility to specify sophisticated cost functions for diverse applications, so long as they can be expressed in terms of the outputs (e.g., images, physics parameters, etc.) with differentiable programming.

**Minimising Specularity:** Intense specular reflections pose one of the greatest challenges to the quality of data gained during an inspection. These regularly cause saturation of the sensor, blooming artifacts, and lens flares which can obscure key elements of interest such as textural and geometric changes. To benchmark  $\partial$ LITE, we formulate a similar cost function to our prior work [17] based on a

Phong reflection model [69] to minimise specular reflections over an inspection period.

Given the modelled surface normals of the target satellite in the world frame  $\hat{\mathbf{n}}$ , and the sun illumination vector  $\hat{\mathbf{l}}$ , we compute the reflection vector  $\hat{\omega}_r$  as,

$$\hat{\omega}_r = 2(\hat{\mathbf{l}} \cdot \hat{\mathbf{n}})\hat{\mathbf{n}} - \hat{\mathbf{l}}. \quad [1]$$

We consider an image  $\mathcal{I} = \{\mathbf{p}_{i,j}, M_{i,j}, \hat{\mathbf{n}}_{i,j}\}$  that is output from our renderer, where  $\mathbf{p}_{i,j}$  represents each pixel,  $M_{i,j}$  is a binary mask for our specific target object, and  $\hat{\mathbf{n}}_{i,j}$  is the normal vector for the surface that the pixel captures. We project out ray vectors for that pixel  $\nu(\mathbf{p}_{i,j})$ , and define a cost function for the specular intensity average over the pixels,

$$\mathcal{L}_S(\mathcal{I}) = \frac{\sum_{i,j} M_{i,j} \max(0, \hat{\omega}_r \cdot \nu(\mathbf{p}_{i,j}))^\alpha}{\sum_{i,j} M_{i,j}}, \quad [2]$$

where  $\alpha$  controls the width of the reflection lobe for the Phong reflection model. We select an  $\alpha$  of 2 in our pipeline to minimise direct reflections without penalising overall illumination across the satellite body.

**Maintaining Imaging Distance:** To ensure optimised relative orbits stay within a suitable imaging distance, we regularise our solution by introducing a distance-based cost. Assuming the initial orbit has a relative distance  $d$  determined acceptable for imaging conditions, we introduce a simple  $L_2$ -loss for each pose,

$$\mathcal{L}_d(r_c, r_t) = (\|r_c - r_t\|^2 - d)^2. \quad [3]$$

We suggest that—depending on desired imaging quality requirements—similar cost functions could be evaluated directly from depth maps from the renderer while remaining differentiable, which would enable better performance for more complex geometries.

## 4. Results and Discussion

### 4.1 Simulating Inspection Missions

We evaluated  $\partial$ LITE by optimising inspection orbits for fictitious spacecraft monitoring each of the following three real-world satellites: Sentinel-6; CloudSat; and the Hubble Space Telescope. We first validated our custom (differentiable) implementation of the SGP4 propagator by comparing it to existing (non-differentiable) implementations of the algorithm from [62]. Figure 5 clearly demonstrates that our implementation closely matches that of [62] over 48 hours of simulation time, with the slight increase in error over time attributed to the accumulation of floating-point inaccuracies.

### 4.2 Trajectory Optimisation and Evaluation

As mentioned in Section 3.1, we optimise the chaser orbit for 200 iterations with an Adam optimiser. We run all

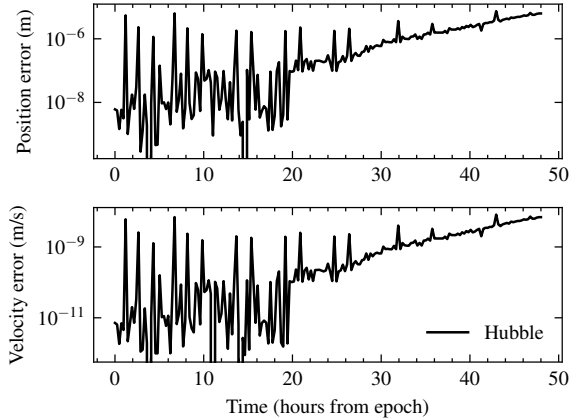


Fig. 5. Comparison of our differentiable SGP4 propagator with existing software [62], using the Hubble Space Telescope as an example. We achieve similar results, with the benefit of our implementation being fully differentiable via JAX [41]. Similar numerical results were observed for CloudSat and Sentinel-6 (not shown).

experiments on a PC with an Intel i9-14900KF, an Nvidia RTX 4090 GPU, and 64GB of memory.

Figure 6 shows the progression of the cost terms over the optimisation process. The curve shows rapid decrease in the total cost with convergence achieved at approximately 100 iterations. We notice that the optimisation trades off deviating from the ideal imaging distance to lower specular costs. This trade off can be tuned by re-weighting  $\lambda_S$  and  $\lambda_d$ . Note also the rapid oscillations in the beginning of the optimisation process which eventually die down. These are indicative of poor conditioning of the cost landscape (e.g., due to deep and long but narrow

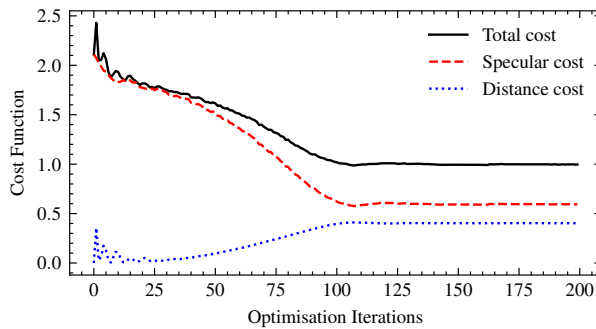


Fig. 6. Total cost, specular cost ( $\mathcal{L}_S$ ), and distance cost ( $\mathcal{L}_d$ ) of the orbital parameters over optimisation iterations for the Hubble Inspection. Our optimisation reaches a local minimum yielding substantially reduced specular cost throughout an orbit.

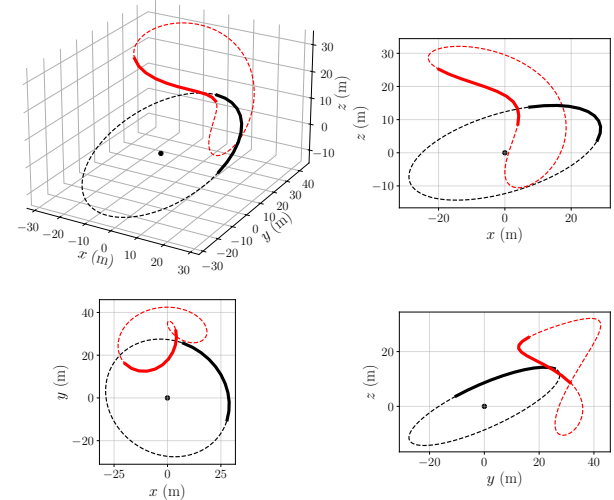


Fig. 7. The orbit of the chaser satellite relative to the target satellite (black dot) in the Hubble inspection experiment. The black circle represents the initialised orbit and red curve represents the optimised orbit. The section of the orbit which the parameters were optimised for ( $t \in [0, T]$ ) are solid, while the rest of the orbit is dashed.

valleys). Visual orbital inspection is particularly prone to this effect, as we may have diverse types of sophisticated cost functions in different units which our decision variables may affect at different scales. For example, a small change in eccentricity or inclination can put the chaser many kilometres away from the target. For this reason, we recommend either manual gradient preconditioning, scaling variables, or first order optimisers which involve some type of adaptive gradient normalisation such as Adam [70].

Figure 7 shows the initial and the final orbits of the chaser in a frame relative to the target satellite, with the inspection period plotted in a solid curve. We notice that while the initial orbit is circular as designed, the final orbit is complex with an inherently 3D structure. It would be non-trivial to manually design such an inspection orbit to optimise the cost, which demonstrates the benefit of our methodology. We note that the inspection period is still approximately close to the desired imaging distance—other parts of the chaser orbit do deviate further from that distance, since they are not directly penalised in our cost function. If desired, this can be easily included by incorporating distance costs over the whole orbit rather than just the inspection period.

Table 2 demonstrates quantitative improvements in visual image quality using the proportion of saturated pixels in the satellite region [13] and the inlier match ratio

Table 2. Visual performance of the proposed optimisation through  $\partial$ LITE. By optimising inspection trajectories,  $\partial$ LITE significantly reduces the proportion of saturated pixels captured in each image and increases the proportion of inlier SIFT feature matches detected. Best values are in bold.

Satellite	Approach	Sat. % ↓	MR↑
HST	Conventional	26.0	0.759
	$\partial$ LITE (Ours)	<b>20.5</b>	<b>0.861</b>
Sentinel-6	Conventional	1.20	0.583
	$\partial$ LITE (Ours)	<b>0.04</b>	<b>0.632</b>
CloudSat	Conventional	5.76	0.614
	$\partial$ LITE (Ours)	<b>2.72</b>	<b>0.801</b>

(MR) as metrics—i.e., inliers of the matched features over the total number of the keypoints detected [71] using SIFT features [72]. We select these metrics as proxies for image quality and 3D reconstruction, respectively. The proposed optimisation approach drastically reduces the proportion of the satellite body which is saturated in the image, whilst also boosting the number of SIFT features detected, compared to the conventional football inspection approach.

In Figure 8 we compare the qualitative results from  $\partial$ LITE at the position of maximum cost. As can be seen, the overall specular cost in the final optimised orbit is significantly lower than that of the initial. Given the complex geometry of the satellite, it is not possible to avoid all specularities over all times, however by optimising across an inspection trajectory the overall impact can be significantly reduced.

To compare how cost minimisation translates to visual fidelity, Figure 9 presents the percentage saturation of pixels observed on the satellite body throughout the orbit until eclipse. The final optimised orbit significantly reduces the proportion of saturated pixels across the inspection mission, validating the proposed specular cost as a viable means to improve image quality.

#### 4.3 Limitations

Currently,  $\partial$ LITE is limited to passive inspection trajectories with full knowledge of the target satellite state. We anticipate that combining variable attitude dynamics of both the target and chaser satellites will enable non-obvious trajectories both in terms of orbital elements and sensor pointing. Moreover, while Mitsuba 3 [16] allows for the customisation of simple pinhole cameras, these models neglect optical distortion, sensor point spread functions, and sensor noise which may be of interest in high-fidelity optical simulations [25]. Motion blur is also neglected, meaning that  $\partial$ LITE can only simulate accu-

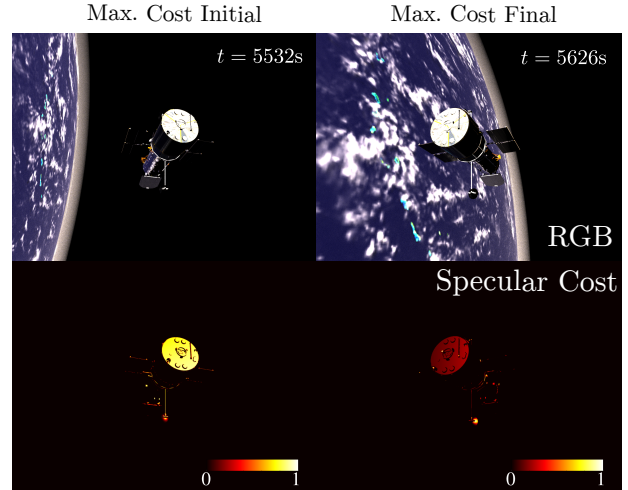


Fig. 8. Qualitative comparison of maximum specular costs observed through an orbit. By optimising orbital parameters to observe the target satellite from different locations and angles, we dramatically reduce specular costs observed through an orbit.

rate fly-by imagery [12] for short exposure times or slow relative motion. Presently, we assume uniform reflection contribution from all materials on the satellite; however, different materials will have wider or narrower specular lobes. Calculating a Phong exponent  $\alpha$  for each material with cost function in Equation 2 would more accurately consider the specularities encountered on-orbit.

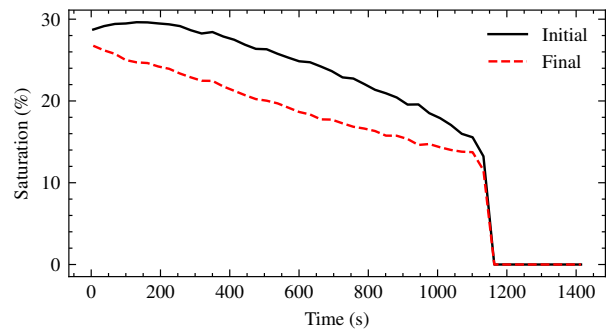


Fig. 9. Percentage of saturated pixels on satellite body during an inspection of Hubble.  $\partial$ LITE minimises our visual reflection cost function which is related to downstream metrics. It can substantially reduce the percentage of pixels which directly reflect sunlight, reducing saturation and thereby improving image quality.

## 5. Conclusions

We have presented  $\partial$ LITE—a fully differentiable pipeline for optimising on-orbit inspection trajectories from visual cost functions. We have demonstrated via simulation that by combining a differentiable rendering engine with a differentiable orbit propagator, we can construct relative inspection trajectories that avoid unfavourable visual features such as specular reflection, thereby improving the quality of captured images.

Future work with  $\partial$ LITE will involve using the pipeline as a design tool for specific on-orbit inspection missions, where we will construct mission-specific cost functions to achieve favourable inspection trajectories. We will also include additional visual costs to minimise shadowing on the spacecraft body. By considering the quality of visual information in the optimisation of inspection trajectories,  $\partial$ LITE achieves non-obvious relative orbits and substantially improved visual observations.

## Acknowledgements

The authors gratefully acknowledge support from the NSW Space Research Network to present this work. This research was supported in part through the NVIDIA Academic Grant Program. This work was supported in part by the ARC Research Hub in Intelligent Robotic Systems for Real-Time Asset Management (IH210100030).

## References

- [1] L. M. Amaya-Mejía, M. Ghita, J. Dentler, M. Olivares-Mendez, and C. Martinez, “Visual servoing for robotic on-orbit servicing: A survey,” in *2024 International Conference on Space Robotics (iSpaRo)*, IEEE, 2024, pp. 178–185.
- [2] T. McMahan, *Repairing solar max: the solar maximum repair mission*. National Aeronautics and Space Administration, Goddard Space Flight Center, 1984, vol. 205.
- [3] National Aeronautics and Space Administration, “Space shuttle mission report: Sts-61 (hubble servicing mission-1),” NASA Johnson Space Center, Tech. Rep., 1994, Accessed: 2025-08-31. [Online]. Available: <https://ntrs.nasa.gov/api/citations/19940015719/downloads/19940015719.pdf>.
- [4] National Aeronautics and Space Administration, “Space shuttle mission report: Sts-82 (hubble servicing mission-2),” NASA Johnson Space Center, Tech. Rep., 1997, Accessed: 2025-08-31. [Online]. Available: <https://www.ibiblio.org/apollo/Shuttle/Reports/Mission%20Reports/STS-82%20Space%20Shuttle%20Mission%20Report.pdf>.
- [5] National Aeronautics and Space Administration, “Space shuttle mission report: Sts-103 (hubble servicing mission-3a),” NASA Johnson Space Center, Tech. Rep., 1999, Accessed: 2025-08-31. [Online]. Available: <https://www.ibiblio.org/apollo/Shuttle/Reports/Mission%20Reports/STS-103%20Space%20Shuttle%20Mission%20Report.pdf>.
- [6] National Aeronautics and Space Administration, “Space shuttle mission report / press kit: Sts-109 (hubble servicing mission-3b),” NASA, Tech. Rep., 2002, Accessed: 2025-08-31. [Online]. Available: <https://www.nasa.gov/wp-content/uploads/2023/05/sts-109-spk-press-kit.pdf>.
- [7] National Aeronautics and Space Administration, “Space shuttle mission report: Sts-125 (hubble servicing mission-4),” NASA Johnson Space Center, Tech. Rep., 2009, Accessed: 2025-08-31. [Online]. Available: <https://www.ibiblio.org/apollo/Shuttle/Reports/Mission%20Reports/STS-125%20Space%20Shuttle%20Mission%20Report.pdf>.
- [8] R. B. Friend, “Orbital express program summary and mission overview,” in *Sensors and Systems for space applications II*, SPIE, vol. 6958, 2008, pp. 11–21.
- [9] S. Tiraplegui *et al.*, “Proba-3: Challenges and needs for sub-millimetre autonomous formation flying,” in *8th European Conference for Aeronautics and Aerospace Sciences (EUCASS)*, 2019. doi: 10.13009/EUCASS2019-764. [Online]. Available: <https://www.eucass.eu/doi/EUCASS2019-0764.pdf>.
- [10] SpaceLogistics LLC (Northrop Grumman), *Mev-1 & mev-2 (mission extension vehicle) overview*, eoPortal – Satellite Missions, Accessed: 2025-09-01, 2025. [Online]. Available: <https://eoportal.org/satellite-missions/mev-1>.
- [11] M. Pyrak and J. Anderson, “Performance of Northrop Grumman’s mission extension vehicle (mev) rpo imagers at geo,” in *Advanced Maui Optical and Space Surveillance Technologies (AMOS) Conference*, Conference paper describing in-orbit sensor performance during rendezvous and proximity operations, Maui, Hawaii, USA, 2021.

- [12] J. Allworth *et al.*, “The use of flyby space-to-space non-earth imagery to rapidly identify and characterise unknown objects,” in *Proceedings of the Advanced Maui Optical and Space Surveillance (AMOS) Technologies Conference*, 2024, p. 51.
- [13] C. L. Gentil *et al.*, “Mixing data-driven and geometric models for satellite docking port state estimation using an rgb or event camera,” *2025 International Conference on Robotics and Automation (ICRA)*, 2025.
- [14] M. Jawaid, E. Elms, Y. Latif, and T.-J. Chin, “Towards bridging the space domain gap for satellite pose estimation using event sensing,” in *2023 IEEE International Conference on Robotics and Automation (ICRA)*, IEEE, 2023, pp. 11 866–11 873.
- [15] D. Vallado, P. Crawford, R. Hujasak, and T. S. Kelso, “Revisiting spacetrack report# 3,” in *AIAA/AAS astrodynamics specialist conference and exhibit*, 2006, p. 6753.
- [16] W. Jakob *et al.*, *Mitsuba 3 renderer*, version 3.0.1, <https://mitsuba-renderer.org>, 2022.
- [17] R. Mishra, J. Naylor, N. H. Barbara, and D. G. Dansereau, “Appearance-aware trajectory optimisation for autonomous on-orbit inspection,” *International Symposium on Artificial Intelligence, Robotics and Automation in Space (i-SAIRAS)*, 2024.
- [18] S. Kitamura, K. Otsubo, T. Chujo, and H. Nakaniishi, “Shadow-aware formation flying using solar radiation pressure with neural network,” in *2024 International Conference on Space Robotics (iSpaRo)*, IEEE, 2024, pp. 210–217.
- [19] R. Zou and S. Bhattacharya, “On optimal pursuit trajectories for visibility-based target-tracking game,” *IEEE Transactions on Robotics*, vol. 35, no. 2, pp. 449–465, 2018.
- [20] S. Xue, J. Dill, P. Mathur, F. Dellaert, P. Tsiotra, and D. Xu, “Neural visibility field for uncertainty-driven active mapping,” in *Proceedings of the IEEE/CVF Conference on Computer Vision and Pattern Recognition*, 2024, pp. 18 122–18 132.
- [21] G. P. Strimel and M. M. Veloso, “Coverage planning with finite resources,” in *2014 IEEE/RSJ International Conference on Intelligent Robots and Systems*, IEEE, 2014, pp. 2950–2956.
- [22] E. Galceran and M. Carreras, “A survey on coverage path planning for robotics,” *Robotics and Autonomous systems*, vol. 61, no. 12, pp. 1258–1276, 2013.
- [23] L. Felicetti *et al.*, “Hysim: A tool for space-to-space hyperspectral resolved imagery,” in *Proceedings of the International Astronautical Congress (IAC)*, IAC-23-D1.4B.11, Baku, Azerbaijan: International Astronautical Federation (IAF), Oct. 2023.
- [24] J. Montalvo, J. I. B. Pérez-Villar, Á. García-Martín, P. Carballeira, and J. Bescós, “Spin: Spacecraft imagery for navigation,” *arXiv preprint arXiv:2406.07500*, 2024.
- [25] M. Pajusalu *et al.*, “Sispo: Space imaging simulator for proximity operations,” *PloS one*, vol. 17, no. 3, e0263882, 2022.
- [26] X. Li, A. Richard, B. C. Yalçın, M. H. Delisle, M. Olivares-Mendez, and C. Martinez, “A modular high-fidelity photorealistic simulator of orbital scenarios: A space debris removal use case,” in *2024 International Conference on Space Robotics (iSpaRo)*, IEEE, 2024, pp. 111–118.
- [27] HEO (High Earth Orbit Robotics Pty Ltd.), *Identification and characterisation of space objects through non-earth imaging*, White Paper, HEO – Non-Earth Imaging (NEI) Technology, Accessed: 2025-09-01, 2025. [Online]. Available: <https://www.heospace.com/resources/white-papers/identification-and-characterisation-of-space-objects-through-non-earth-imaging>.
- [28] J. A. E. Agency, *CRD2 Phase I/ADRAS-J update: “fixed-point observation” images of space debris have been released*, [https://global.jaxa.jp/press/2024/06/20240614-2\\_e.html](https://global.jaxa.jp/press/2024/06/20240614-2_e.html), Accessed: 2025-08-31, Jun. 2024.
- [29] M. Rasotto *et al.*, “Differential algebra space toolbox for nonlinear uncertainty propagation in space dynamics,” 2016.
- [30] B. Addis, A. Cassioli, M. Locatelli, and F. Schoen, “A global optimization method for the design of space trajectories,” *Computational Optimization and Applications*, vol. 48, no. 3, pp. 635–652, 2011.
- [31] M. Vasile, E. Minisci, and M. Locatelli, “Analysis of some global optimization algorithms for space trajectory design,” *Journal of Spacecraft and Rockets*, vol. 47, no. 2, pp. 334–344, 2010.
- [32] R. P. Russell, “Survey of spacecraft trajectory design in strongly perturbed environments,” *Journal of Guidance, Control, and Dynamics*, vol. 35, no. 3, pp. 705–720, 2012.
- [33] J. E. Prussing, *Optimal spacecraft trajectories*. Oxford University Press, 2018.

- [34] B. Bernhard, C. Choi, A. Rahmani, S.-J. Chung, and F. Hadaegh, "Coordinated motion planning for on-orbit satellite inspection using a swarm of small-spacecraft," in *2020 IEEE Aerospace Conference*, 2020, pp. 1–13. doi: 10.1109/AERO47225.2020.9172747.
- [35] S. M. LaValle, *Planning Algorithms*. Cambridge University Press, 2006, Available at <http://planning.cs.uiuc.edu/>.
- [36] B. E. Jackson, K. Tracy, and Z. Manchester, "Planning with attitude," *IEEE Robotics and Automation Letters*, vol. 6, no. 3, pp. 5658–5664, 2021.
- [37] T. A. Howell, B. E. Jackson, and Z. Manchester, "Altro: A fast solver for constrained trajectory optimization," in *2019 IEEE/RSJ International Conference on Intelligent Robots and Systems (IROS)*, IEEE, 2019, pp. 7674–7679.
- [38] D. C. Woffinden, "On-orbit satellite inspection : Navigation and [Delta]v analysis," Thesis, Massachusetts Institute of Technology, 2004. (visited on 09/05/2025).
- [39] M. Blondel and V. Roulet, "The elements of differentiable programming," *arXiv preprint arXiv:2403.14606*, 2024.
- [40] J. Bezanson, A. Edelman, S. Karpinski, and V. B. Shah, "Julia: A fresh approach to numerical computing," *SIAM Review*, vol. 59, pp. 65–98, 1 2017. doi: 10.1137/141000671. [Online]. Available: <https://epubs.siam.org/doi/10.1137/141000671>.
- [41] J. Bradbury *et al.*, *JAX: Composable transformations of Python+NumPy programs*, 2018. [Online]. Available: <https://github.com/google/jax>.
- [42] T. A. Howell, K. Tracy, S. Le Cleac'h, and Z. Manchester, "Calipso: A differentiable solver for trajectory optimization with conic and complementarity constraints," in *The International Symposium of Robotics Research*, Springer, 2022, pp. 504–521.
- [43] R. S. Sutton and A. G. Barto, *Reinforcement Learning: An Introduction*, Second. The MIT Press, 2018, ISBN: 9780262039246. [Online]. Available: <http://incompleteideas.net/book/the-book-2nd.html>.
- [44] A. Paszke *et al.*, "Pytorch: An imperative style, high-performance deep learning library," *Advances in neural information processing systems*, vol. 32, 2019.
- [45] T. A. Howell, S. L. Cleac'h, J. Z. Kolter, M. Schwager, and Z. Manchester, "Dojo: A differentiable simulator for robotics," Mar. 2022. doi: 10.48550/arxiv.2203.00806. [Online]. Available: <https://arxiv.org/abs/2203.00806v2>.
- [46] M. Mittal *et al.*, "Orbit: A unified simulation framework for interactive robot learning environments," *IEEE Robotics and Automation Letters*, vol. 8, no. 6, pp. 3740–3747, 2023. doi: 10.1109/LRA.2023.3270034.
- [47] C. D. Freeman, E. Frey, A. Raichuk, S. Girgin, I. Mordatch, and O. Bachem, "Brax – a differentiable physics engine for large scale rigid body simulation," *arXiv preprint arXiv:2106.13281*, Jun. 2021. [Online]. Available: <https://arxiv.org/abs/2106.13281v1>.
- [48] M. Nimier-David, D. Vicini, T. Zeltner, and W. Jakob, "Mitsuba 2: A retargetable forward and inverse renderer," *Transactions on Graphics (Proceedings of SIGGRAPH Asia)*, vol. 38, no. 6, Dec. 2019. doi: 10.1145/3355089.3356498.
- [49] H. Kato *et al.*, "Differentiable rendering: A survey," *arXiv preprint arXiv:2006.12057*, 2020.
- [50] M. Pharr, W. Jakob, and G. Humphreys, *Physically based rendering: From theory to implementation*. MIT Press, 2023.
- [51] S. Laine, J. Hellsten, T. Karras, Y. Seol, J. Lehtinen, and T. Aila, "Modular primitives for high-performance differentiable rendering," *ACM Transactions on Graphics*, vol. 39, no. 6, 2020.
- [52] M. Jawaid, M. Märtens, and T.-J. Chin, "Event-rbg fusion for spacecraft pose estimation under harsh lighting," *arXiv preprint arXiv:2507.05698*, 2025.
- [53] E. Todorov, T. Erez, and Y. Tassa, "Mujoco: A physics engine for model-based control," in *2012 IEEE/RSJ International Conference on Intelligent Robots and Systems*, IEEE, 2012, pp. 5026–5033. doi: 10.1109/IROS.2012.6386109.
- [54] R. Tedrake and the Drake Development Team, *Drake: Model-based design and verification for robotics*, 2019. [Online]. Available: <https://drake.mit.edu>.
- [55] M. Z. Irshad *et al.*, "Neural fields in robotics: A survey," *arXiv preprint arXiv:2410.20220*, 2024.
- [56] J. Michaux *et al.*, "Let's make a splan: Risk-aware trajectory optimization in a normalized gaussian splat," *IEEE Transactions on Robotics*, 2025.

- [57] M. G. Andreu, V. Klemm, V. Patil, J. Tordesillas, and M. Hutter, “Foci: Trajectory optimization on gaussian splats,” *arXiv preprint arXiv:2505.08510*, 2025.
- [58] A. Shirazi, J. Ceberio, and J. A. Lozano, “Evolutionary algorithms to optimize low-thrust trajectory design in spacecraft orbital precession mission,” in *2017 IEEE Congress on Evolutionary Computation (CEC)*, 2017, pp. 1779–1786. doi: 10.1109/CEC.2017.7969517. [Online]. Available: <https://ieeexplore.ieee.org/document/7969517/>.
- [59] G. Acciarini, A. G. Baydin, and D. Izzo, “Closing the gap between sgp4 and high-precision propagation via differentiable programming,” *Acta Astronautica*, vol. 226, pp. 694–701, 2025, ISSN: 0094-5765. doi: <https://doi.org/10.1016/j.actaastro.2024.10.063>. [Online]. Available: <https://www.sciencedirect.com/science/article/pii/S0094576524006374>.
- [60] F. R. Hoots and R. L. Roehrich, “Spacetrack report no. 3: Models for propagation of NORAD element sets,” Aerospace Defense Center, Peterson Air Force Base, Tech. Rep., 1980.
- [61] *Fundamentals of astrodynamics and applications*. Springer Science & Business Media, 2001, vol. 12.
- [62] B. Rhodes, *Python-sgp4*, 2018. [Online]. Available: <https://github.com/brandon-rhodes/python-sgp4>.
- [63] C. Wehrli, “Extraterrestrial solar spectrum,” Physikalisch-Meteorologisches Observatorium and World Radiation Center, Davos Dorf, Switzerland, Tech. Rep. Publication No. 615, Jul. 1985.
- [64] T. Zhang, P. W. Stackhouse Jr, B. Macpherson, and J. C. Mikovitz, “A solar azimuth formula that renders circumstantial treatment unnecessary without compromising mathematical rigor: Mathematical setup, application and extension of a formula based on the subsolar point and atan2 function,” *Renewable Energy*, vol. 172, pp. 1333–1340, 2021.
- [65] D. W. Hughes, B. Yallop, and C. Hohenkerk, “The equation of time,” *Monthly Notices of the Royal Astronomical Society*, vol. 238, no. 4, pp. 1529–1535, 1989.
- [66] R. Stöckli, E. Vermote, N. Saleous, R. Simmon, and D. Herring, “The blue marble next generation: A true color earth dataset including seasonal dynamics from modis,” NASA Earth Observatory / NASA Goddard Space Flight Center, Tech. Rep. BMNG Dataset Documentation, Oct. 2005, PDF documentation of the Blue Marble Next Generation (BMNG) dataset. [Online]. Available: <https://assets.science.nasa.gov/content/dam/science/esd/eo/content-feature/bluemarble/bmng.pdf>.
- [67] D. Vicini, S. Speierer, and W. Jakob, “Path replay backpropagation: Differentiating light paths using constant memory and linear time,” *ACM Transactions on Graphics (TOG)*, vol. 40, no. 4, pp. 1–14, 2021.
- [68] J. R. Schott, *Remote Sensing: The Image Chain Approach*, 2nd ed. New York: Oxford University Press, 2007, ISBN: 978-0-19-517817-3.
- [69] B. T. Phong, “Illumination for computer generated pictures,” in *Seminal graphics: pioneering efforts that shaped the field*, 1998, pp. 95–101.
- [70] D. P. Kingma and J. L. Ba, “Adam: A method for stochastic optimization,” in *3rd International Conference on Learning Representations*, International Conference on Learning Representations, ICLR, 2015.
- [71] J. L. Schonberger, H. Hardmeier, T. Sattler, and M. Pollefeys, “Comparative evaluation of hand-crafted and learned local features,” in *Proceedings of the IEEE conference on computer vision and pattern recognition*, 2017, pp. 1482–1491.
- [72] D. G. Lowe, “Distinctive image features from scale-invariant keypoints,” *International journal of computer vision*, vol. 60, no. 2, pp. 91–110, 2004.